Received: 7 December 2021 | Revised: 22 February 2022 | Accepted: 15 March 2022

DOI: 10.1111/ejss.13233

ORIGINAL ARTICLE

European Journal of Soil Science WILEY

Response of subsoil organic matter contents and physical properties to long-term, high-rate farmyard manure application

Frederic Leuther[1] | **Maximilian Wolff**[2] | **Klaus Kaiser**[2] | **Lena Schumann**[2] | **Ines Merbach**[3] | **Robert Mikutta**[2] | **Steffen Schlüter**[1]

[1]Department of Soil System Science, Helmholtz Centre for Environmental Research – UFZ GmbH, Halle (Saale), Germany

[2]Soil Science and Soil Protection, Martin Luther University Halle-Wittenberg, Halle (Saale), Germany

[3]Department of Community Ecology, Helmholtz Centre for Environmental Research – UFZ GmbH, Experimental Station, Bad Lauchstädt, Germany

Correspondence
Frederic Leuther, Department of Soil System Science, Helmholtz Centre for Environmental Research – UFZ GmbH, 06120, Halle (Saale), Germany.
Email: frederic.leuther@ufz.de

Maximilian Wolff, Soil Science and Soil Protection, Martin Luther University Halle-Wittenberg, 06120, Halle (Saale), Germany.
Email: maximilian.wolff@landw.uni-halle.de

Funding information
This research has been supported by the Deutsche Forschungsgemeinschaft (grant no. 416883305).

Abstract

Application of farmyard manure (FYM) is common practice to improve physical and chemical properties of arable soil and crop yields. However, studies on effects of FYM application mainly focussed on topsoils, whereas subsoils have rarely been addressed so far. We, therefore, investigated the effects of 36-year FYM application with different rates of annual organic carbon (OC) addition (0, 469, 938 and 1875 g C m^{-2} a^{-1}) on OC contents of a Chernozem in 0–30 cm (topsoil) and 35–45 cm (subsoil) depth. We also investigated its effects on soil structure and hydraulic properties in subsoil. X-ray computed tomography was used to analyse the response of the subsoil macropore system (≥19 μm) and the distribution of particulate organic matter (POM) to different FYM applications, which were related to contents in total OC (TOC) and water-extractable OC (WEOC). We show that FYM-C application of 469 g C m^{-2} a^{-1} caused increases in TOC and WEOC contents only in the topsoil, whereas rates of ≥938 g C m^{-2} a^{-1} were necessary for TOC enrichment also in the subsoil. At this depth, the subdivision of TOC into different OC sources shows that most of the increase was due to fresh POM, likely by the stimulation of root growth and bioturbation. The increase in subsoil TOC went along with increases in macroporosity and macropore connectivity. We neither observed increases in plant-available water capacity nor in unsaturated hydraulic conductivity. In conclusion, only very high application of FYM over long periods can increase OC content of subsoil at our study site, but this increase is largely based on fresh, easily degradable POM and likely accompanied by high C losses when considering the discrepancy between OC addition rate by FYM and TOC response in soil.

Highlights

- A new image processing procedure to distinguish fresh and decomposed POM.
- The increase of subsoil C stock based to a large extend on fresh, labile POM.

Frederic Leuther and Maximilian Wolff authors contributed equally to this study.

- Potential of arable subsoils for long-term C storage by large FYM application rates is limited.
- The increase in TOC has no effect on hydraulic properties of the subsoil.

KEYWORDS

carbon stock, carbon storage, hydraulic properties, particulate organic matter, plant available water content, X-ray computer tomography, soil structure

1 | INTRODUCTION

Soil is a major reservoir of carbon (C) and plays an important role in regulating atmospheric CO_2 (Batjes, 2014; Chen et al., 2019; Robinson, 2007; Scharlemann et al., 2014). One way of using the potential of agroecosystems as C sink is by making full use of the soil C storage capacity (Lal, 2018). The application of C-rich amendments, such as farmyard manure (FYM), is a well-established practice to enhance crop yields and increase soil organic carbon (OC) stocks on the long term. In their meta-analysis including 101 studies with different manure application treatments and agricultural systems, Gross and Glaser (2021) showed that OC stocks increased on average by 37% in topsoils (0–20 cm) and 26% in subsoils (>20 cm) upon an average manure application rate of 37.4 Mg ha^{-1} a^{-1}. However, the increase was highly dependent on manure type, management system and soil properties, such as texture, acidity and initial C content.

In long-term field experiments under conventional tillage, the effects of FYM application on subsoil C contents are inconsistent. For example, Ghosh et al. (2018) showed that 44 years of FYM application with 263 g C m^{-2} a^{-1} in combination with NPK fertilisation significantly increased the soil OC content by about 20% down to 90 cm depth. In contrast, Liang et al. (2012) observed only in topsoils significant increases in soil OC stocks after 15 years of FYM application (324 g C m^{-2} a^{-1}). The deep placement of OC is, however, one mechanism to substantially increase its mean residence time in soil due to limitations in oxygen supply, reduced accessibility for decomposers and formation of stabile mineral–organic associations (Dungait et al., 2012; Ekschmitt et al., 2008; Rumpel & Kögel-Knabner, 2011). The main pathways of OC input into subsoils are identified as root litter and root exudates, dissolved organic matter and/or bioturbation, but their relative importance depends on the environmental conditions and management practices on site (Rumpel & Kögel-Knabner, 2011). In long-term field studies, the focus is often on combinations of different fertilisers optimised for adequate nutrient supply rather than on different application rates of FYM. To the best of our knowledge, so far, no studies addressed possible threshold values of FYM-C addition rates above which enrichment of OC occurs not only in topsoil but also in subsoil.

Manure and plant residues, mainly representing coarse particulate organic matter (POM), are typically applied at the surface and then, mixed into the topsoil (upper 0–30 cm) by ploughing. Major pathways for FYM-C into deeper soil layers include the vertical translocation of POM by bioturbation (Angst et al., 2019) and leaching of dissolved organic matter (as DOC), the latter been considered the most mobile form of organic matter in soil (Kaiser & Kalbitz, 2012). An increase of OC is not only relevant to the built-up of C reservoir in soil but also for improving soil structure and water retention.

In arable topsoils, soil structure development is mainly driven by field management practices, which regularly cause reshaping and mixing of structural components and creation of large macropores (Dal Ferro et al., 2014; Jarvis et al., 2017; Schlüter et al., 2018). Incorporation of POM, such as plant residues in FYM, into soil promotes aggregation and porosity (Bhattacharyya et al., 2007; Grosbellet et al., 2011; Six et al., 2004). Application of FYM for more than 5 years has been shown to result in greater total porosity, aggregate stability, saturated hydraulic conductivity and water retention capacity of differently textured topsoils, mostly along with increases in OC contents (Benbi et al., 1998; Bhattacharyya et al., 2007; Ozlu et al., 2019; Singh et al., 2021). Zhang et al. (2021) showed that 150 years of FYM application (35 Mg ha^{-1} a^{-1}) more than doubled the soil OC content of a clay-loam topsoil and, as revealed by X-ray micro-computer tomography (μCT), significantly increased the visible porosity as well as the permeability of the pore networks of aggregates and soil columns. This was confirmed by X-ray μCT studies on a fine-loamy topsoil receiving of FYM (16 Mg ha^{-1} a^{-1}) for 10 years (Singh et al., 2021) and a silt-loam topsoil after 50 years of FYM (60 Mg h^{-1} a^{-1}) application (Dal Ferro et al., 2013).

As in topsoils, also in subsoils, structure and macropore architecture are actively shaped by biological activity (Jarvis, 2007; Rabot et al., 2018). Here, biopores

created by root growth and faunal activity contribute most to soil macroporosity (Lucas et al., 2019). At the same time, biopores support direct OC input of plant and fauna residues to deeper soil layers (Rumpel et al., 2012). Gajri et al. (1994) showed that in addition to mineral NPK fertilisation, application of FYM not only increased the maize biomass production above ground but also resulted in increased root growth. Deep roots and their exudates are therefore another pathway for OC into the subsoil, which can be affected by FYM application. It was further determined that FYM can cause a significant decrease in subsoil bulk density due to accumulation of low-density organic matter (Ghosh et al., 2018; Schjønning et al., 1994) and by inducing greater activity of deep burrowing earthworms (Andersen, 1983). The creation of new pores by stimulated bioactivity and an increasing amount of soil OC, especially of porous and hydrophilic POM, can positively affect soil hydraulic properties, such as plant available water capacity (Hudson, 1994). In summary, FYM application promotes bioturbation, root growth and accumulation of soil OC, but studies exploring the impact of variable FYM rates on OC levels and, furthermore, on physical soil properties in subsoil are scarce.

X-ray μCT is a powerful tool to characterise the soil structure of undisturbed samples and to analyse the spatial environment of its constituents. New image processing protocols enable the segmentation and classification of POM according to their morphological properties (Elyeznasni et al., 2012; Juyal et al., 2021; Schlüter et al. 2022). In this study, we combined soil physical analyses and X-ray μCT imaging with the chemical characterisation of soil OC to distinguish between different C forms, that is, μCT-derived estimates of POM fractions classified according to their morphological properties, organic matter embedded in the soil matrix based on μCT-determined density information and concentrations of soil OC forms, such as total OC (TOC) and water-extractable OC (WEOC).

The aims of our study were to explore the long-term effect of increasing FYM application rates on structure, hydraulic properties and chemical characteristics beneath the plough horizon and to quantify different forms of subsoil OC in response to FYM application rates and relate it to OC characteristics in topsoil layers in order to identify different entry pathways of C into the subsoil. The following hypotheses were tested:

1. The expected increase in vertical C translocation with increasing FYM rates results in proportional increases in subsoil C content.
2. The expected increase in C alters the soil structure also in the subsoil.
3. Enhanced macroporosity and OC content increase the unsaturated hydraulic properties of the subsoil.

2 | MATERIALS AND METHODS

2.1 | Study site and sampling

The soil in Bad Lauchstädt, Germany, is a Haplic Chernozem developed from quaternary loess (Altermann et al., 2005). The investigated soil layer at 35–45 cm depth was characterised by a silt loam texture (9% sand, 70% silt, 21% clay) and TOC and total nitrogen (TN) contents of 11.2 and 1.1 g kg^{-1}. Illite, kaolinite and vermiculite are the dominant phyllosilicate minerals of the clay fraction (Dreibrodt et al., 2002).

The long-term field trial was established in 1983 to study the effect of increased application rates of FYM (0, 50, 100 and 200 Mg ha^{-1} a^{-1}) on crop yield, crop quality and soil fertility (Franko & Schulz, 2021; Körschens et al., 1994). It was designed as a two-factorial block experiment in two replicates (Figure 1a), with the first factor being FYM application rate and the second one being land use (cropped or bare fallow). For replicate a, the plots were arranged according to increasing manure application rate; replicate b was randomised. The design of the long-term field trial v494 does not include physical barriers between plots so that carry-over of manure during ploughing to neighbouring plots in the randomised replicates as well as a systematic even out in replicate a cannot entirely be ruled out. Therefore, we only used the 0 Mg ha^{-1} a^{-1} plot of replicate a as control and avoided the area close to the next plot for sampling. This study is based on the cropped plots only, to include C inputs from roots and plant residues, and the soil structural formation by plants in response to manure application. The individual size for cropped plots was 64 m^2, and FYM was applied every year in autumn before ploughing. The FYM from cattle farming had an average dry matter content of 25.2 weight% with TOC and TN contents of 37.2% and 2.9%. The annual C input by FYM results in addition rates of 0, 469, 938 and 1,875 g m^{-2} a^{-1} (Franko & Schulz, 2021). Over time, the crop rotation changed from sugar beet – silage maize – winter weed (1984–1989), sugar beet – potato – silage maize (1990–2007), potato – sugar beet – silage maize (2008–2013) and potato (2014) to silage maize (since 2015).

Sampling of undisturbed soil cores at 35–45 cm depth and of disturbed soil samples for C characterisation from 0–45 cm was done in March 2020 and 2021, respectively. From each plot, two 250 cm^3 cylinders (r = 4 cm, h = 5 cm) and three 21 cm^3 cylinders (r = 1.5 cm and h = 3 cm) were taken within an area of 1.5 m^2 to gain in total 10 replicates

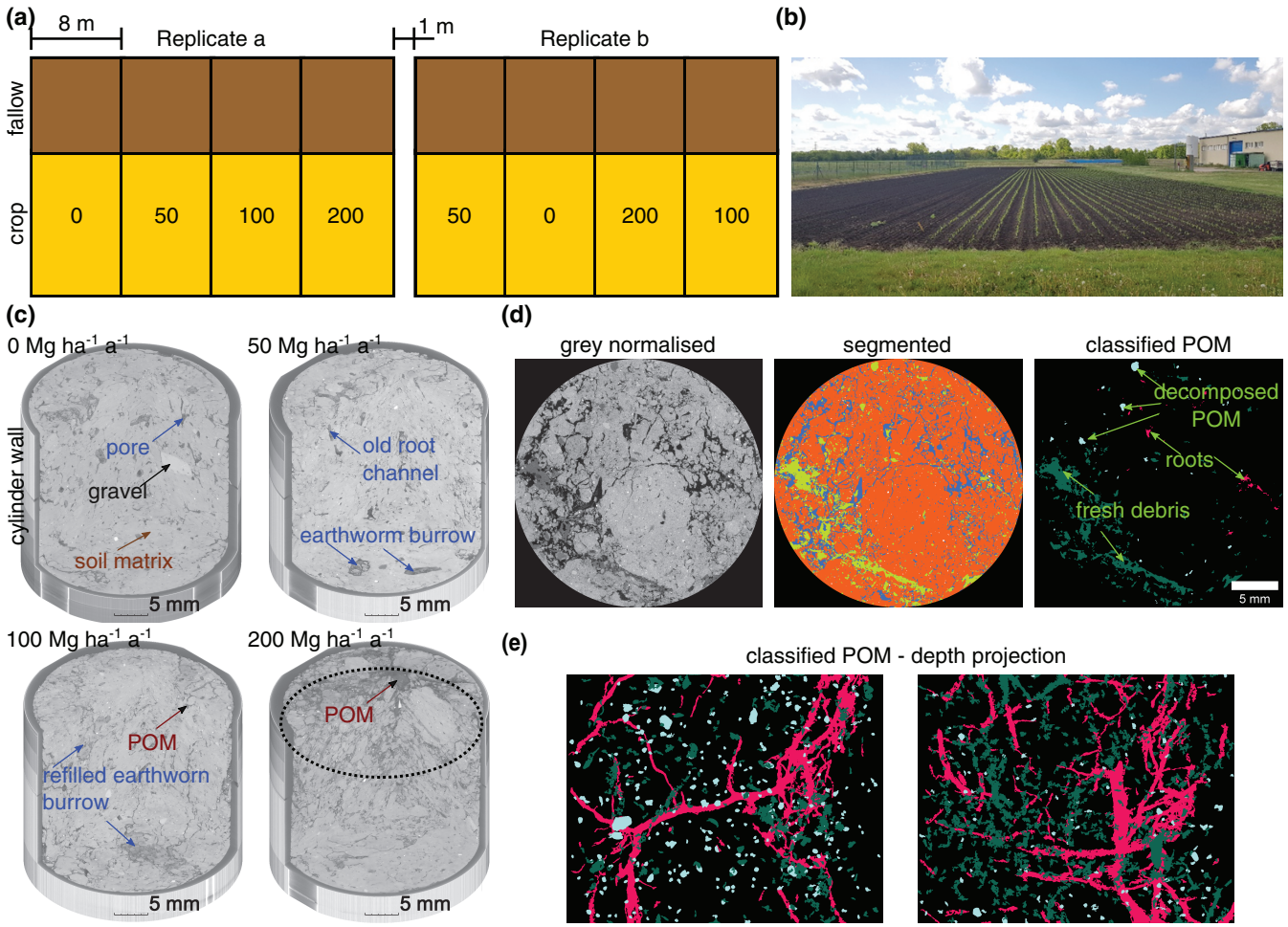

FIGURE 1 Plot design of the field experiment (a), the field site in spring 2020 1 month after sampling (b), a representative 21-cm^3 µCT image of every treatment (c), the dashed circle marks the area of the 2D slight as a representative for the image processing workflow as shown in (d) and (e) shows the depth projections of two classified µCT images where white represents decomposed particulate organic matter (POM), green fresh debris and pink roots

per manure application rate. Disturbed samples were taken with a gauge auger (r = 1.75 cm) at three different locations per plot and separated into depth increments from 0–25 cm, 25–35 cm and 35–45 cm. The three samples taken per plot and depth were homogenised to mixed samples of around 330 g air dried weight per depth.

2.2 | Chemical soil properties

Following sampling, stones and larger plant residues were removed by sieving to <2 mm, and the material was dried at 40 °C. Soil pH was measured potentiometrically in duplicates in the supernatant of a suspension containing 10 g soil and 25 ml 0.01 M $CaCl_2$ after 5 min on a horizontal shaker and 60 min sedimentation. The soil reaction was circumneutral in all treatments, with pH values between 7.4 (0 Mg ha^{-1} a^{-1}) and 7.0 (200 Mg ha^{-1} a^{-1}). Contents of Fe, Al and Si largely present in mineral components were determined by ammonium-oxalate extraction (Schwertmann, 1964) and dithionite-citrate-bicarbonate extraction (Mehra & Jackson, 1960). Element concentrations in extraction solutions were analysed by inductively coupled plasma optical emission spectroscopy (ICP-OES; Ultima 2, Horiba Jobin-Yvon, France). Differences in elements indicative of the mineral composition were minimal between plots (Table 2), suggesting a fairly homogeneous parent material. For all samples, the mean oxalate-extractable Fe, Al and Si contents were 1.27 ± 0.01, 1.07 ± 0.02 and 0.32 ± 0.00 g kg^{-1}, and Fe_d accounted for 5.71 ± 0.04 g kg^{-1}.

The TC and TN contents were determined for all samples in triplicates by dry combustion using a Vario EL Cube (Elementar Analysesysteme GmbH, Germany). All samples were free of inorganic C; therefore, the determined C contents were assumed to represent TOC. The

TOC and TN stocks in 35–45 cm depth were calculated by Equation (1):

$$\text{stock} = \text{content} \times \text{bulk density} \times \text{depth} \times \text{surface area factor} \times 0.001, \quad (1)$$

where TOC and TN stock are expressed as g m^{-2}, TOC and TN content as g kg^{-1}, bulk density as g cm^{-3}, depth as 10 cm layer and surface area factor as 10,000 cm^2 m^{-2}.

WEOC and total N (WETN) were determined in 8 g soil suspended in 40 ml deionised water at 20°C (Surey et al., 2020). Samples were shaken for 10 min (50 agitations per min) and stored for 18 h in the dark. After centrifugation (3000 *g*) for 10 min, the supernatant was passed through a 0.45-µm membrane filter (Supor-450, Pall Cooperation, United States) and analysed for C and N contents (multi N/C® 3100, Analytik Jena, Jena, Germany). Contents of NO_3^- and NH_4^+ (N_{min}) were determined with a Continuous-Flow Analyser (ScanPlus, Skalar Analytical B.V., Netherlands). WEON was calculated by the difference of WETN and N_{min}. The specific UV absorbance ($SUVA_{280}$) as an estimate of aromaticity of WEOC was determined by measuring the UV absorbance at 280 nm (SPECORD 210 PLUS, Analytik Jena AG, Germany) and normalising it to the WEOC concentration.

2.3 | Soil hydraulic properties

Water retention and unsaturated hydraulic conductivity were measured with a HYPROP device (METER Group, Inc. USA) for a potential range from 0 to −5,000 hPa using the evaporation method (Schindler et al., 2010). Soil samples (250 cm^3) were slowly saturated with water from the bottom for 24 hours. At the end, soil samples were dried at 105 °C to calculate dry mass, bulk density, total porosity and air capacity. Soil water retention below −10,000 hPa was determined for mixed subsamples of 4 g soil using a WP4C instrument (METER Group, Inc. USA) with two replicates per sample and three measurement points per sample. The hydraulic conductivity and water content at field capacity (pF 1.8), the permanent wilting point (PWP; pF 4.2) and the plant-available water capacity (PAWC), that is, the difference between water content at pF 1.8 and pF 4.2, were calculated based on a bimodal van Genuchten model as implemented in the HYPROP-fit software.

2.4 | Soil structure and POM classification

Imaging was done with an industrial X-ray µCT device (X-TEK XTH 225, Nikon Metrology, Belgium). The 250 cm^3 samples were scanned for 47 min at 150 kV and 310 µA using a 0.7-mm copper filter for beam hardening reduction, resulting in 2000 projections (0.708 s per projections, 2 frames per projection). A voxel resolution of 50 µm was achieved at an 8-bit greyscale resolution in the reconstructed tomogram. The 21-cm^3 samples were scanned for 63 min at 130 kV and 150 µA using a 0.1-mm copper filter, likewise resulting in 2,000 projections (0.708 s per projections, 2 frames per projection) and reconstructed with a voxel resolution of 19 µm (8-bit format). A representative reconstruction of a 21-cm^3 sample of every treatment is shown in Figure 1c.

Image processing and analysis were done with the software packages Ilastik pixel classification (Berg et al., 2019), FIJI ImageJ V1.53 (Schindelin et al., 2012) and R Studio (R Core Team, 2020). The pore system of the larger soil cores was classified via simple thresholding following the image processing steps as described by Schlüter et al. (2016). Images were filtered with a nonlocal means filter (Buades et al., 2011), and pore segmentation was carried out based on the threshold selection method of Otsu (1979). At the coarse resolution, segmentation of organic material as a third class was not possible. Small plant residues were classified as pores. The 21-cm^3 soil samples were segmented via Ilastik pixel classification (https://www.ilastik.org), an interactive tool based on machine learning. Here, a random forest classifier is trained on the original structure by the user for different pixel classes attributes, such as grey value and intensity gradients. The workflow for image segmentation and POM classification is illustrated in Figure 1d and described in the following: Before image segmentation, the grey values of the µCT images were normalised between the cylinder wall and quartz in order to reduce the variance in grey values between images. Then, a training data set for Ilastik pixel classification of 10 subvolumes (400 × 400 × 400 voxel) were selected from different samples where all structural features observed in the µCT images were represented. Based on the training dataset, the samples were segmented into pores, POM, soil matrix and dense material with an out-of-bag (OOB) estimate of error rate of 3.8%.

The classification of segmented POM into roots, fresh debris and decomposed POM was based on their morphological characteristics. POM is known to change its structural appearance with residence time in soil (Elyeznasni et al., 2012; Juyal et al., 2021; Schlüter et al. 2022). Fresh roots are typically coherent, elongated objects; fresh debris has a fragmented structure with large surface area, while decomposed POM becomes more compact and rounded as it ages in soil. At first, the POM class was filtered with a median 3D filter to fill holes and remove isolated POM voxels. Second, a connected component labelling was done for POM clusters >6.86×10^{-3} mm^3 (1000 voxels) with the MorphoLibJ plugin (Legland et al., 2016). Third, different

TABLE 1 Morphological traits of particulate organic matter objects used for random forest classification into decomposed particulate organic matter, roots and fresh debris (modified from Schlüter et al. 2022)

Trait	Definition	Remark
Blobness	$R_3/\sqrt{R_2R_1}$	Objects are described as equivalent inertia ellipsoids with radii $R_3 > R_2 > R_1$. The larger R_3 in comparison to the other, the less elongated the object is.
Compactness	$V/\frac{4}{3}\pi R_1R_2R_3$	The more compact, that is, bulkier with less holes, the more similar the real volume V is to the volume of an equivalent ellipsoid.
Sphericity	$36\pi V^2/A^3$	The sphericity index is defined as the ratio of the squared volume over the cube of the surface area A, normalised such that the value for a ball equals one.
Plateness	$\lvert R_2\rvert/\lvert R_1\rvert$	In plate-like objects R_2 is much larger than R_1 (and more similar to R_3).

shape and volume properties of the segmented POM clusters in every sample were determined by the MorphoLibJ plugin (Legland et al., 2016) and stored in a separate text file. The labelled shape properties of the single components were transferred into R Studio and used to calculate further morphological characteristics typical for roots, fresh debris and decomposed POM. The characteristics are described in detail in Table 1; an example is given in the Data S1 (Table S1). A training data set with 910 observations was created by manually assigning POM clusters to the three POM classes. The remaining 96,900 observations were classified based on the shape properties of the training data set with a random forest classifier in R (Liaw & Wiener, 2002) as follows: The training data set was split into two subsets for training ($n = 637$) and validation ($n = 273$). A classifier was trained with 500 trees and two variables followed by a new classifier trained on all available data ($n = 910$), resulting in an OOB estimate of error rate at 18.4%. Combining roots and fresh debris into one class of fresh POM reduced the OOB estimate of error rate to 7.1%. The subclassification of fresh POM into debris and roots resulted in an OOB error of 14%. Repeated randomised subsampling ($n = 7$, Table S2) provided a good estimate of the volume fractions of roots and fresh debris and associated errors. The results gained by the classifier were assigned to the labelled POM image with MorpholibJ (Figure 1e). The classified POM image was used to calculate the size distribution of the three POM classes with the Local Thickness method in FIJI ImageJ, as well as the distance of each POM particle to the next pore.

The volumetric POM information gained by X-ray CT was re-calculated into a gravimetric C concentration (g C kg^{-1} soil) by the measured bulk densities and the assumption that POM has a density of 1.2 g cm^{-3} and C content of 40% independent of the POM age (Golchin et al., 1994; Kaiser et al., 2002; Mikutta et al., 2019; Moody & Worrall, 2017). This calculation enabled to evaluate the maximum contribution of the image-derived POM to TOC, including POM >2 mm. The difference between POM and TOC was used as an estimate of mineral-associated organic matter (MAOM), including POM particles smaller then resolution. The segmented soil matrix was used to measure the mean matrix grey value in the normalised images. Differences in grey values are the results of differences in material density and therefore enable to capture differences in the matrix composition below the detection limit.

The segmented pore classes at both resolutions, 19 and 50 μm, were analysed according to the typical pore characteristics, which are described in detail in Vogel et al. (2010) and Weller et al. (2021). The visible macroporosity, the distance between voxels classified as pores, the pore size distribution and two different pore connectivity characteristics were determined with Fiji ImageJ. The pore size distribution was computed for both resolution by the maximum-inscribed sphere method with a minimum pore size of 2 voxel, and the frequency distribution of pores sizes was calculated by the first derivative of the combined cumulative pore size distribution [vol.-% mm^{-1}] (Vogel et al., 2010). The connectivity of the pore network was described by the connection probability (Γ) and the Euler number density (χ). The dimensionless Γ-indicator reflects the probability of two randomly chosen pore voxels to belong to the same pore cluster (Renard & Allard, 2013) and was calculated by Equation (2):

$$\Gamma(p) = \frac{1}{n_p^2}\sum_{i=1}^{N(X_p)} n_i^2, \tag{2}$$

where n_p is the total number of pore voxels in the analysed volume, X_p, and n_i is the number of pore voxels per cluster. The χ value was calculated with the MorphoLibJ plugin (Legland et al., 2016) and quantifies the connectivity as the number of isolated pores minus the number of redundant connections plus the number of cavities, expressed as a density [mm^{-3}]. The same plugin was used to determine the pore surface density [mm^{-2}]. The frequency distribution of pore sizes, pore distances and POM sizes were used to calculate their average sizes and distances as weighted means.

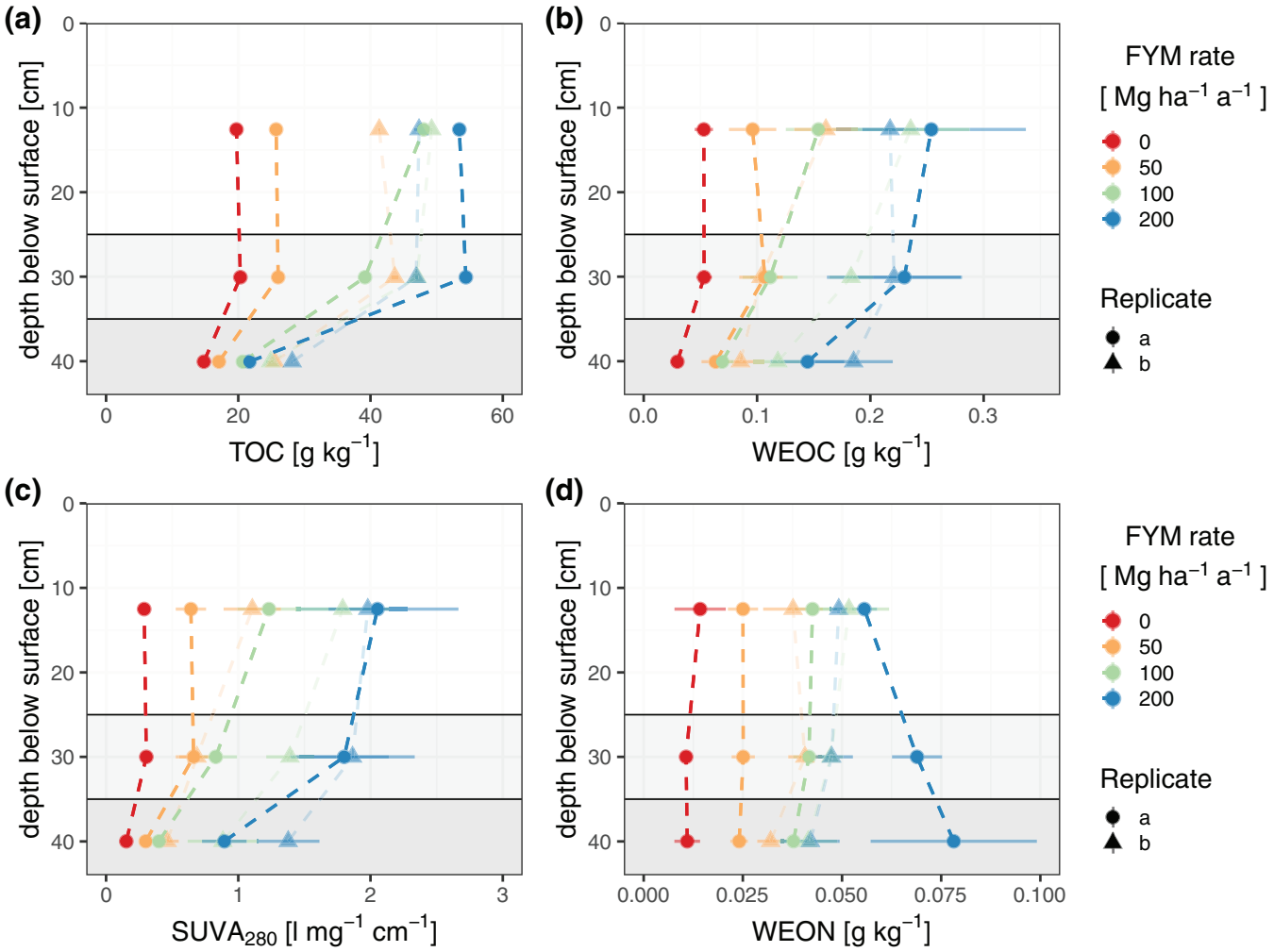

FIGURE 2 Depth profiles of (a) total organic C (TOC), (b) water extractable organic C (WEOC), (c) specific UV absorbance at 280 nm ($SUVA_{280}$) and (d) water-extractable organic N (WEON). The different grey values in the background mark the sampling depths for the mixed sample from 0–25 cm (plough horizon), 25–35 cm (plough pan) and 35–45 cm (horizon of interest). The error bars mark two times standard error of 4 measurements. The results of replicate b were affected by farmyard manure (FYM) carryover and therefore presented in transparent colour shades

2.5 | Statistical analysis

Data management, data analysis and figures were done using the open source packages tidyverse (Wickham et al., 2019) and ggplot2 (Wickham, 2016) in R Version 4.0.2 (R Core Team, 2020). The comparisons of means for each soil property were done using a two-way ANOVA in the rstatix package (Kassambara, 2020). Parameters were tested for normality and homogeneity of variance for each time point by the Shapiro–Wilk test and Levene's test, respectively. The significance was tested by a Kruskal–Wallis test with Bonferroni p-adjustment as implemented in the agricolae package (de Mendiburu, 2019), when the requirements for an ANOVA were not fulfilled. The regressions and correlation coefficients, R^2 and p value, were determined using the ggpubr package (Kassambara, 2020).

3 | RESULTS

3.1 | Chemical characterisation of organic matter in topsoil and subsoil

The contents of TOC, WEOC, WEON, as well as $SUVA_{280}$ of WEOC increased with FYM application rate at all depths studied. The increases were most systematic in the non-randomised plots of replicate a, with reduced effects of manure carryover (Figure 2a–d). Within the uppermost 25 cm, application of FYM systematically

increased the TOC content, with application of 200 Mg ha^{-1} a^{-1} more than doubling the TOC content from 19.7 g kg^{-1} (control) to 53.5 g kg^{-1}. Interestingly, except for the 100 Mg ha^{-1} a^{-1} treatment with a slight decrease in TOC content, there were no differences in TOC contents between the plough horizon (0–25 cm) and the plough pan (25–35 cm). Beneath 35 cm, the TOC decreased significantly compared to the plough horizon for all treatments (control = 14.8 g kg^{-1}, 200 Mg ha^{-1} a^{-1} = 24.9 g kg^{-1}), most strongly for FYM application rates ≥100 Mg ha^{-1} a^{-1}. The absolute differences between TOC contents at the different FYM application rates were greatest in the plough horizon and smallest in the subsoil. In contrast, the decrease in WEOC with depth was less pronounced, and WEON was not affected by depth. The increase in $SUVA_{280}$ with FYM application rate at all depths reflects a higher aromaticity of WEOC; nevertheless, for each FYM rate, $SUVA_{280}$ was lower in the subsoil than in the topsoil (Figure 2c).

In the subsoil of replicate a, the application of 50, 100 and 200 Mg FYM ha^{-1} a^{-1} increased the TOC content by factor 1.2, 1.4 and 1.6 (Figure 2a) and TN by factor 1.2, 1.4 and 1.8 (Figure S1a), respectively. WEOC and WEON represented only about 1%–3% of TOC and TN, with the effect of FYM application rate on the water-extractable fractions and aromaticity being most evident at 35–45 cm. Compared to the control, the different rates of FYM increased the WEOC content by factor 2.1, 2.3 and 4.8, the aromaticity of WEOC by factor 2.0, 2.6 and 5.9 and WEON content by factor 2.2, 3.4 and 7.1. The impact of FYM application on N contents along the profile affected the C/N ratio. With increasing FYM application, the TOC/TN ratio

TABLE 2 Mean physicochemical parameters in 35–45 cm depth in response to long-term farmyard manure (FYM) application rate

	0 Mg ha^{-1} a^{-1} ***n* = 2**	**50 Mg ha^{-1} a^{-1}** ***n* = 4**	**100 MMg ha^{-1} a^{-1}** ***n* = 4**	**200 Mg ha^{-1} a^{-1}** ***n* = 4**	***p*-value**
Bulk density [g cm^{-3}]	1.56 (0.06)^{a}	1.42 (0.04)^{a}	1.40 (0.03)^{a}	1.39 (0.03)^{a}	0.080
Air capacity [vol.-%]	9.41 (2.33)^{a}	13.3 (1.39)^{a}	15.1 (1.81)^{a}	15.8 (1.74)^{a}	0.198
Field capacity [vol.-%]	31.7 (0.24)^{a}	33.1 (0.44)^{a}	32.1 (0.68)^{a}	31.8 (0.95)^{a}	0.506
Wilting point [vol.-%]	15.0 (0.62)^{a}	13.9 (0.55)^{a}	14.4 (0.40)^{a}	15.4 (0.85)^{a}	0.369
PAWC [vol.-%]	16.8 (0.39)^{a}	19.3 (0.82)^{a}	17.7 (0.44)^{a}	16.4 (0.81)^{a}	0.061
k at field capacity [cm d^{-1}]	0.06 (0.00)^{a}	0.38 (0.22)^{a}	0.16 (0.03)^{a}	0.14 (0.02)^{a}	0.393
pH [−]	7.4 (0.02)^{a}	7.3 (0.17)^{a}	7.0 (0.09)^{b}	7.0 (0.04)^{b}	0.022
	***n* = 4**	***n* = 8**	***n* = 7**	***n* = 8**	
Fe_d [g kg^{-1}]	5.83 (0.06)^{a}	5.89 (0.07)^{a}	5.72 (0.05)^{a}	5.48 (0.07)^{b}	<0.001
Fe_o [g kg^{-1}]	1.26 (0.05)^{a}	1.21 (0.02)^{a}	1.31 (0.02)^{a}	1.28 (0.03)^{a}	0.092
Al_o [g kg^{-1}]	1.15 (0.02)^{a}	1.17 (0.03)^{a}	1.05 (0.01)^{b}	0.98 (0.01)^{c}	<0.001
Si_o [g kg^{-1}]	0.39 (0.01)^{a}	0.33 (0.01)^{ab}	0.31 (0.01)^{bc}	0.28 (0.02)^{c}	0.002
TOC [g kg^{-1}]*	16.90 (0.08)^{a}	16.82 (0.56) ^{a}	24.67 (1.44)^{b}	33.72 (1.49)^{c}	<0.001
TN [g kg^{-1}]	1.34 (0.01)^{a}	1.36 (0.07)^{a}	2.19 (0.14)^{b}	3.17 (0.15)^{c}	<0.001
TOC/TN [−]	12.65 (0.07)^{a}	12.40 (0.20) ^{a}	11.21 (0.07)^{b}	10.63 (0.09)^{c}	<0.001
	***n* = 3**	***n* = 6**	***n* = 6**	***n* = 6**	
Visible porosity [vol.-%]	7.06 (0.63)^{a}	8.29 (0.68)^{ab}	8.94 (0.98)^{ab}	11.4 (0.66)^{b}	0.014
Mean pore size [mm]	0.15 (0.01)^{a}	0.11 (0.01)^{a}	0.14 (0.02)^{a}	0.14 (0.03)^{a}	0.669
Mean pore distance [mm]	0.14 (0.00)^{a}	0.11 (0.00)^{ab}	0.11 (0.01)^{ab}	0.09 (0.01)^{b}	<0.001
Surface density [mm^{-1}]	2.37 (0.10)^{a}	3.17 (0.17)^{ab}	3.22 (0.29)^{ab}	4.05 (0.26)^{b}	0.005
Euler number χ [mm^{-3}]	6.41 (3.44)^{a}	9.12 (9.95)^{a}	14.80 (3.75)^{a}	22.20 (6.13)^{a}	0.466
Γ-connectivity [−]	0.66 (0.06)^{a}	0.65 (0.05)^{a}	0.72 (0.06)^{a}	0.76 (0.03)^{a}	0.380
Matrix grey value	164 (0.24)^{a}	160 (1.09)^{ab}	157 (1.17)^{ab}	155 (1.74)^{b}	0.004
Fresh POM [vol.-%]	0.28 (0.12)^{a}	0.54 (0.08)^{a}	1.67 (0.32)^{b}	4.03 (0.96)^{c}	0.001
Decomposed POM [vol.-%]	0.06 (0.01)^{a}	0.05 (0.01) ^{a}	0.20 (0.02) ^{b}	0.33 (0.04)^{b}	<0.001

Note: Parameter of X-ray μCT analysis is the results of the 21-cm^3 samples. Fresh POM is the sum of volumetric roots and fresh debris contents. Values in parentheses are standard errors, letters and *p*-value represent statistical significance of ANOVA and Kruskal–Wallis tests. *Soil layer was free of inorganic carbon.

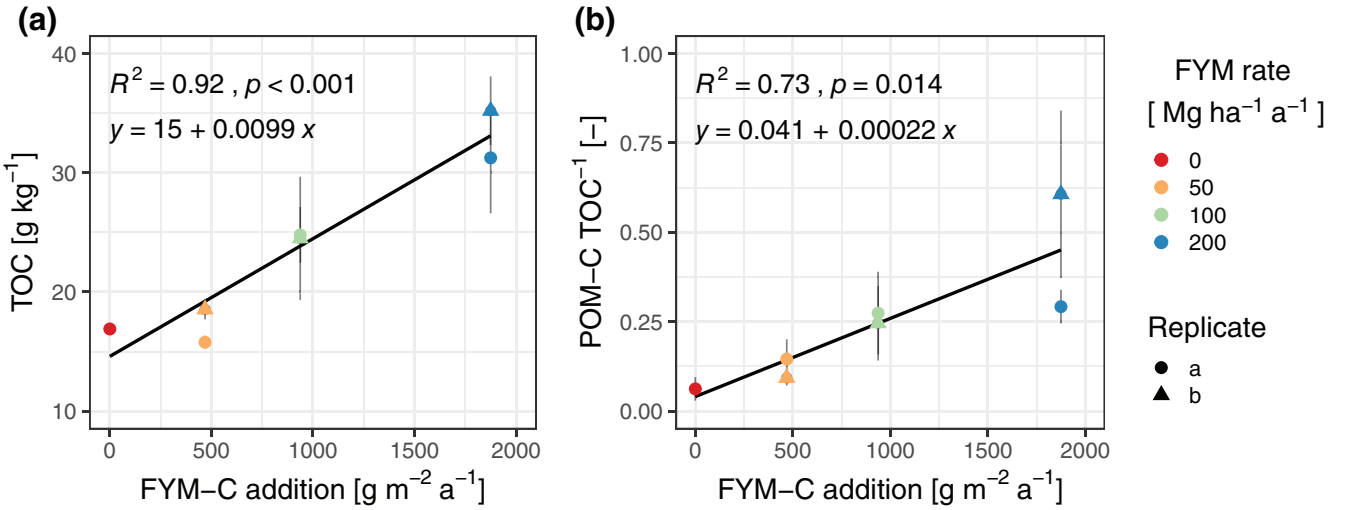

FIGURE 3 Total organic carbon (TOC, a) and ratio between particulate organic matter (POM)-C and TOC (b) in 35–45 cm depth as function of annual carbon addition by farmyard manure application. Dots mark the mean values per plot, error bars depict two times the standard error

became narrower and differences within a treatment along the soil profile smaller (Figure S1b).

Table 2 presents the TOC and TN contents measured for the undisturbed soil cores taken from 35–45 cm depth in 2020. The contents were in accordance with those measured in 2021 (Figure 2a and S1a). The FYM plots, including the results of replicate b, show a high variability in data compared to the control, likely due to the described manure carryover in replicate b. No significant differences in TOC and TN between the control and the 50 Mg ha^{-1} a^{-1} plots were observed but for FYM application rates ≥100 Mg ha^{-1} a^{-1} TOC and TN were significantly increasing (Table 2). Figure 3a shows that the TOC content in subsoil significantly increased with FYM-C addition rate ($R^2 = 0.92$, $p < 0.001$) from 16.8 to 24.6 g kg^{-1} (100 Mg ha^{-1} a^{-1}) and 33.7 g kg^{-1} (200 Mg ha^{-1} a^{-1}). A similar significant correlation ($R^2 = 0.92$, $p < 0.001$) was found for TN, where an increase from 1.3 to 3.3 g kg^{-1} (200 Mg ha^{-1} a^{-1}) was observed. Thirty-six years of different FYM application rates resulted in total C addition of 0, 16,884 (50 Mg ha^{-1} a^{-1}), 33,768 (100 Mg ha^{-1} a^{-1}) and 67,500 (200 Mg ha^{-1} a^{-1}) g C m^{-2}. Compared to the control (2636 g C m^{-2}), the C stock per m^2 in the analysed 10 cm subsoil layer was slightly decreasing for the 50 Mg ha^{-1} a^{-1} plots (2388 g C m^{-2}) and increasing for the 100 Mg ha^{-1} a^{-1} plots (3454 g C m^{-2}) and 200 Mg ha^{-1} a^{-1} plots (4688 g C m^{-2}). Thus, only 2.4% (100 Mg ha^{-1} a^{-1}) and 3.0% (200 Mg ha^{-1} a^{-1}) of the FYM C addition might have reached the analysed subsoil layer. The total N addition of 0, 1315, 2,630 and 5261 g N m^{-2} during 36 years resulted in N stocks of 209 g N m^{-2} (control), 193 g N m^{-2} (50 Mg ha^{-1} a^{-1}), 307 g N m^{-2} (100 Mg ha^{-1} a^{-1}) and 441 g N m^{-2} (200 Mg ha^{-1} a^{-1}). Also for TN, the stock was slightly decreasing for the lowest FYM input rate; 3.7% and 4.4% of the applied N might have reached the analysed subsoil layer for the higher FYM input rates.

3.2 | Source and distribution of particulate organic matter in arable subsoil

In subsoil, the majority of the determined POM objects were classified as fresh POM, i.e., roots and fresh debris. The volume fraction of fresh POM increased significantly with FYM rate ($R^2 = 0.59$, $p < 0.001$; Table 2). The mean volume fraction of fresh POM ranged between <1% and 4% and scaled linearly with FYM rate. In the control plots, fresh POM was dominated by roots, shares of root-type and fresh debris POM were about equal in the 50 Mg ha^{-1} a^{-1} plots, while for the plots, ≥100 Mg ha^{-1} a^{-1} most fresh POM was classified as fresh debris (Table S2). Both, volumes of roots and fresh debris were increasing with FYM application rate, but fresh debris rather exponentially and roots linearly. The variability within the classification and herewith the risk of misclassification was also increasing with FYM application rate. The volume fraction of decomposed POM was about 10 times smaller than that of fresh POM, but again a significant increase was observed with increasing FYM application ($R^2 = 0.72$, $p < 0.001$). The maximum contribution of image-derived POM-C to TOC contents was 6% in the control, 12% in the 50 Mg ha^{-1} a^{-1} plots, 25% at 100 Mg ha^{-1} a^{-1} plots and 45% at the 200 Mg ha^{-1} a^{-1} plots (Figure 3b, $R^2 = 0.73$, $p = 0.014$). The 200 Mg ha^{-1} a^{-1} plots of replicate b show a high variability in POM-C

due to large differences in fresh POM-C. The relation of fresh (R^2 = 0.83, $p < 0.01$) and decomposed POM (R^2 = 0.92, $p < 0.001$) to TOC was even closer than to FYM-C addition rate (Figure 4a,b, Figure 3a), that is, when the carryover effect is directly accounted for. Thus, in the following, the TOC content was used as a reference value

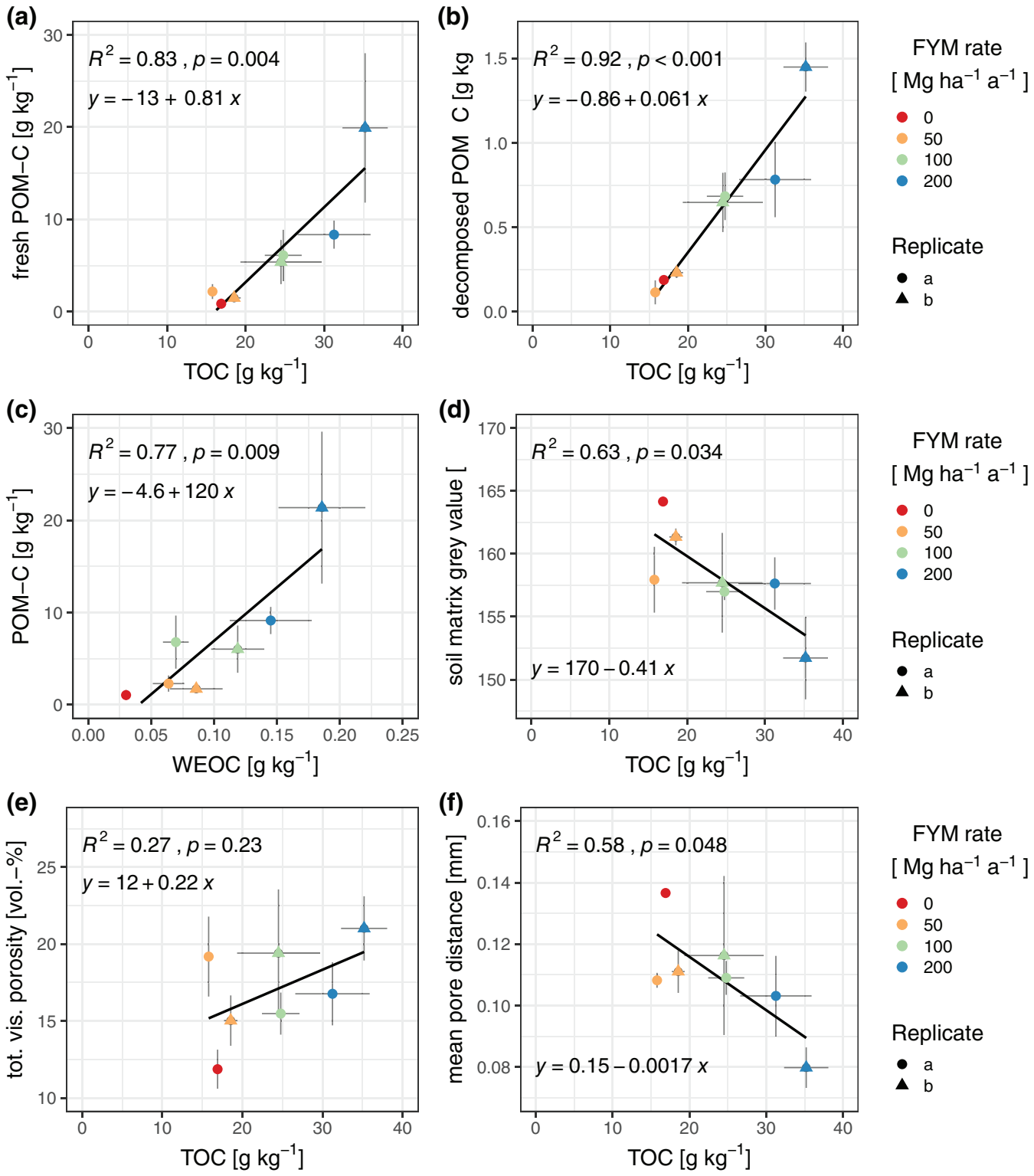

FIGURE 4 Fresh (a) and decomposed particulate organic matter (POM)-C (b) determined via µCT as a function of total organic C (TOC) and water extractable organic C (WEOC) (c). (d) shows the mean grey value of the normalised soil matrix as a function of TOC. The total visible porosity (e) was determined as a combined porosity measurement at both resolutions, that is, 19 and 50 µm. The mean distance of voxels classified as matrix to the next pore (f) was determined at a resolution of 19 µm. Dots mark the mean values per plot; error bars depict two times the standard error

for the degree of effect of FYM on the subsoil. There was also a correlation between C in all visible POM and WEOC ($R^2 = 0.77$, $p < 0.01$, Figure 4c), although less strong. Again, no significant differences in fresh and decomposed POM contents were observed between the lowest FYM rate (50 Mg ha^{-1} a^{-1}) and control in the subsoil. The mean grey value of the soil matrix, an indicator of density changes due to the accumulation of soil organic matter smaller than the resolution limit and an increase in sub-resolution porosity, decreased with increasing TOC content ($R^2 = 0.63$, $p = 0.034$, Figure 4d).

Image-based POM classification further enabled to analyse the spatial location of POM in the undisturbed soil (Figure 5c) and the determination of POM-specific diameters (Figure 5b). Including all treatments, POM classified as decomposed had significantly ($p < 0.001$) larger mean distances to the next pore (85 µm) compared to fresh POM (roots = 46 µm, fresh debris = 51 µm). Volumes of POM classified as roots had a diameter range of 38–800 µm, with a mean root diameter of 180 µm. Most particles classified as decomposed POM had a narrower diameter range of 110–230 µm. For fresh debris (38–1,400 µm), the measurement of the particle diameter was not an ideal description of the size due to fragmentation and holes, which is reflected by the large error bars of the individual measurement points (Figure 5b).

3.3 | Soil structure and hydraulic properties in subsoil

In subsoil, differences in structural parameters were mainly found between control and the FYM plots but not between the different application rates (Table 2) due to rather high variability. The subsoil of the control was in total denser and had a reduced total visible porosity (1.56 g cm^3, 11.9 vol.%) compared to the FYM treatments (1.34–1.48 g cm^3, 15.0–21.0 vol.%). When using the TOC as an indicator for FYM impact on single plots, differences became more obvious. The structure parameters determined for the 21-cm^3 samples show that an increase in TOC content causes an increase in connection probability Γ from 0.64 to 0.79 ($R^2 = 0.69$, $p = 0.021$), where Γ close to 1 indicates a well-connected pore system. In contrast, the Euler number density χ indicated poor connectivity ($\chi > 0$) in all treatments, and was even increasing with TOC content ($R^2 = 0.55$, $p = 0.057$). Thus, pore networks were not fully interconnected, but the probability of a well-connected pore system increased with TOC content. The mean pore distances in soil decreased ($R^2 = 0.58$, $p = 0.048$, Figure 4f) with increasing TOC content, while pore surface densities increased ($R^2 = 0.71$, $p = 0.017$). Both results suggest that the added

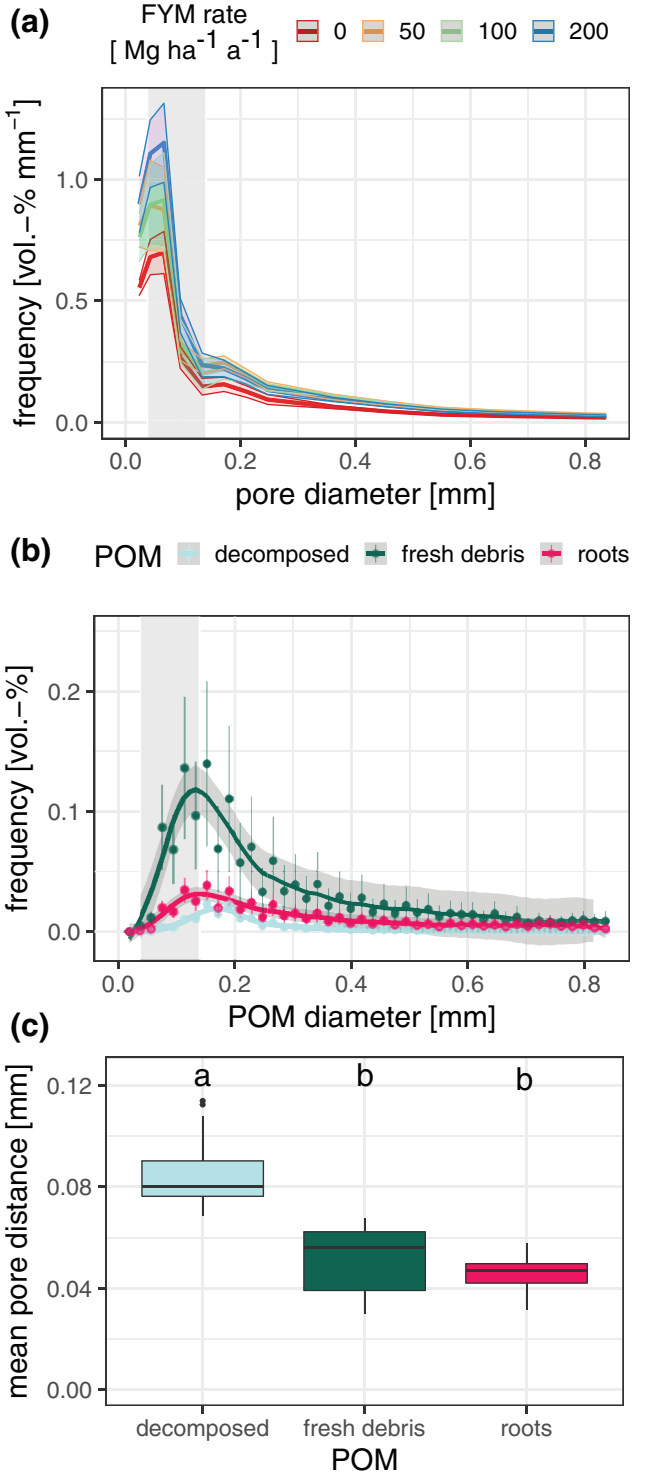

FIGURE 5 Frequency distribution of pore diameters (a) as a result of combined porosity measurements at both resolutions, i.e., 19 µm and 50 µm. The frequency distribution in particulate organic matter (POM) diameters (b) and mean pore distance of different POM classes (c) represent the mean value of 24 measurements per POM type. The shaded areas of the pore frequency distributions and the whiskers in (a) and (b) mark two times the standard error. The letters in (c) represent statistical significance of ANOVA. The grey backgrounds in (a) and (b) mark the pore diameter range were the frequencies differ between (FYM) application rates

POM also contributed more pore surfaces. The visible porosity of the 21 cm^3 samples was significantly increasing with TOC ($R^2 = 0.85$, $p = 0.003$). When combining the pore size distribution of both resolutions, including also larger macropores, the correlation between TOC and the total visible porosity became less strong ($R^2 = 0.27$, $p = 0.23$, Figure 4e). Likewise, the correlation between matrix grey value and TOC ($R^2 = 0.63$, $p = 0.034$, Figure 4d) or bulk density and TOC ($R^2 = 0.19$, $p = 0.335$) was weaker, that is, when all non-visible pores or all pores were considered, respectively. These varying degrees of explained variability suggest that a small range of macropore diameters was affected most by additional C accumulation. Therefore, the combined PSD was analysed according to differences in certain pore size ranges. The increase in total visible porosity for FYM treatments compared to control occurred over a broad range of pore sizes (0.04–1.20 mm), but significant differences between FYM treatments were only found up to 0.14 mm (Figure 5a) with 200 Mg ha^{-1} a^{-1} plots having the highest frequency. Interestingly, the mean diameters determined for POM correspond to the diameter range of 0.12–0.25 mm, which is close to where pore volumes differed most significantly between FYM rates.

Table 2 shows that neither air capacity nor the field capacities at pF 1.8 and the PWP at pF 4.2 in the subsoils were correlated to FYM application rate, as were the overall water retention curves (Figure S2a). The difference between field capacity and PWP resulted in PAWCs between 16.4 and 19.3 vol.%. Neither the differences in bulk density ($R^2 = 0.07$, $p = 0.37$, Figure S2c), visible macroporosity of the soil cores ($R^2 = 0.13$, $p = 0.20$), nor TOC contents ($R^2 = 0.25$, $p = 0.07$, Figure S2e) significantly affected PAWC below the plough pan, since the variation in PAWC was small. In addition, differences in TOC content due to FYM application rates had no effect on the unsaturated hydraulic conductivity for matrix potentials ranging from pF 1.8 to 3.5 (Table 2, Figure S2b). At field capacity, the hydraulic conductivity was decreasing with decreasing bulk density ($R^2 = 0.48$, $p < 0.01$) and visible macroporosity ($R^2 = 0.41$, $p < 0.01$), but no correlation was determined to TOC ($R^2 = 0.0$, $p = 0.862$, Figure S2f). For the hydraulic conductivity at lower matrix potential (>pF 2), no correlations were found with measured structural and chemical parameters.

4 | DISCUSSION

4.1 | Long-term FYM application enhances subsoil organic carbon storage

After 36 years of FYM application, we found that soil OC contents not only increased in topsoil but also in subsoil beneath the plough horizon. This is a novel finding as previous results obtained at the same site after only 9 years of FYM application merely observed a significant TOC increase in topsoil (Körschens et al., 1994). However, the effect of additional 25 years of FYM application on subsoil TOC contents was only detected for the FYM application rates of 100 and 200 Mg ha^{-1} a^{-1}, corresponding to additions of 938 and 1,875 g C m^{-2} a^{-1}. Here, the subsoil TOC contents increased by 45% and 100% compared to the control, respectively. The calculation of the total amount of C stored in the subsoil layer (35–45 cm depth) showed that the C stocks of plots with 100 and 200 Mg ha^{-1} a^{-1} FYM application increased by about 31% (817 g C m^{-2}) and 78% (2,050 g C m^{-2}). These amounts equate to only about 2% to 3% of the total amount of FYM-C applied to the topsoil over 36 years (33,768 and 67,500 g m^{-2}). The sight decrease in C-stocks at the 50 Mg ha^{-1} a^{-1} plots was due to the decrease in bulk density while C concentration remained constant. The increase in C stocks is in contrast to the meta-analysis by Gross and Glaser (2021), where average C stocks in subsoils (>20 cm) already increased by 26% by an average manure application of 37.4 Mg ha^{-1} a^{-1}. However, the meta-analysis also showed that soils with high sand contents responded stronger to FYM application than fine-textured soils, especially when initial TOC contents were low.

The pH value, clay content, land use management and form of applied manure were identified as additional factors for increases in soil OC upon FYM application. Wiesmeier et al. (2019) further emphasise the role of metal oxides as sorbents of OC. The little variation in mineral composition between plots, however, suggests that the observed differences in OC content in our study can be directly attributed to the different FYM application rates. Using the 50 Mg ha^{-1} a^{-1} plots as reference, the increase in C input with increasing rates of FYM application did not result in a concomitant increase in subsoil OC contents. This means that, on average, a fourfold increase in FYM supply only doubled the SOC content in the subsoil. Compared to the plough horizon, the increase in TOC was generally smaller. After 36 years of FYM application at the study site, the determined rate of FYM-C addition needed to induce significant increases in subsoil OC content was ≥938 g C m^{-2} a^{-1} (FYM rate ≥ 100 Mg ha^{-1} a^{-1}), which is far higher than rates commonly used in agriculture. We cannot say whether a significant increase in subsoil OC content may arise eventually in the 50 Mg ha^{-1} a^{-1} plots, when continued for more than 36 years.

4.2 | Increase in subsoil organic carbon storage based to a large extend on fresh POM

A more detailed analysis of the organic matter fractions allowed differentiation between the forms and sources that

contributed to the increase in subsoil OC contents. The new image analysis protocol not only enabled us to segment POM and distinguish it according to morphological properties into fresh and decomposed POM but also to calculate the contribution of POM to TOC based on volumetric information. The analysis of intact soil cores by X-ray μCT also allowed for determining the position of different POM classes with respect to pore distances and thus to infer the occlusion state of the POM. For plots with comparable low TOC content (control and 50 Mg ha^{-1} a^{-1}), visible POM contributed 6.2%–14.6% to the TOC content. With increasing TOC content, the contribution of POM to TOC increased to 26.0% (100 Mg ha^{-1} a^{-1}) and 45.0% (200 Mg ha^{-1} a^{-1}) mainly due to the increase in fresh POM. Visible roots dominated the fresh POM class in the control and both, volumes of roots and fresh debris, were increasing with FYM application rate. Fresh debris increased rather exponentially and roots linearly, leading to a dominant proportion of fresh debris in the high FYM plots. The stimulation of root growth by FYM application is in accordance with previous studies (Gajri et al., 1994; Masood et al., 2014; Shahzad et al., 2014). Bad Lauchstädt is regularly affected by dry periods, which may have additionally stimulated root growth in subsoil (Comas et al., 2013), especially if there is a sufficient nutrient supply and low mechanical resistance due to reduced subsoil density (de Moraes et al., 2019). There is a fuzzy transition of detectable root and fresh debris because roots will become morphologically indistinguishable from fresh debris when they lose their cylindrical shape due to emergence of branched structures or due to fragmentation into smaller pieces. Root origin of fresh debris might explain its appearance in the control but not the significant increase in the FYM plots ≥100 Mg ha^{-1} a^{-1}. Furthermore, fresh debris contained POM with diameters larger than those determined for roots, which excludes maize roots as potential source of larger POM pieces. Although the input of plant residues and manure by ploughing is primary limited to the topsoil, Chernozems are well known for bioturbation due to megafauna, such as earthworms and small vertebrates, which can transports POM to deeper soil layers (Altermann et al., 2005; Angst et al., 2019; Schjønning et al., 1994). The positive correlations between TOC, macroporosity, connectivity and mean pore distance indicate stimulation of biological activity upon FYM application and increase the possibility for POM being transferred to the subsoil.

The substantial contribution of fresh POM to TOC increase suggests that most of the POM beneath the plough pan has entered the subsoil only recently and might become mineralised rapidly. However, since this surplus in fresh POM enters the subsoil every year it might have contributed to steady built-up of less degradable POM still visible 6 months after harvest. POM classified as decomposed POM was predominately located in areas with greater distances to pores >19 μm and thus, suggest occlusion within the soil matrix. Occlusion of POM by denser materials of reduced connection to the main pore network is a mechanism known to protect POM from microbial decomposition (Golchin et al., 1994; Lehmann & Kleber, 2015). The stimulation of root growth by FYM application increased OC input and the development of pores in a range between 30 and 150 μm (grey background in Figure 5), the most active zone for microbial activity. Microbial degradation products that become released during the degradation of POM can diffuse into the neighbouring soil matrix and be stabilised (Kravchenko et al., 2019; Witzgall et al., 2021).

The content of WEOC in topsoil was affected by the amount of FYM applied, but the contribution of WEOC to TOC was rather low (1%–3%). In subsoil, the strong correlation of WEOC to POM suggests that the increase in WEOC was most likely released from the additional POM sources and not by DOC input from the upper soil layers. The remaining 90% (control and 50 Mg ha^{-1} a^{-1}), 74% (100 Mg ha^{-1} a^{-1}) and 55% (200 Mg ha^{-1} a^{-1}) of TOC, which were not related to fresh and decomposed POM, likely represent mineral-associated organic matter (MAOM) with calculated OC concentrations of 15.4, 18.2 and 18.0 g kg^{-1}. The results of the control and lowest input rate were in line with previous studies at the same site using density fractionation where about 80 to 95% of OC was assigned to MAOM (John et al., 2005; Surey et al., 2020). The gradual increase in MAOM was also reflected in a decrease in soil matrix density. Overall, these findings suggest that the subsoil mineral phase in the studied Chernozem soil was either already saturated with organic matter or incapable of binding additional OC under the neutral pH conditions regardless the amount of applied FYM. The lack of proportional MAOM formation may thus indicate that the potential of agricultural subsoils for being used as C sinks in response to increased biomass input depends much on environmental site conditions, including soil type and climatic conditions.

4.3 | Minor effect of long-term FYM application on physical and hydraulic subsoil properties

Overall, the increase in subsoil TOC by increasing application rates of FYM promoted a well-connected macropore system in the subsoil. The increase in pore surface densities and the decrease in matrix–pore distances with increasing TOC contents indicate stimulated bioturbation and/or soil loosening upon increasing POM accumulation. Changes in visible porosity occurred in pore sizes range from 38–140 μm. The very different degrees of correlation between contrasting pore sizes (all pores, sub-resolution pores

<40 μm, narrow macropores >40 μm, larger macropores >140 μm) and TOC indicate that narrow macropores benefit most from the biopore formation by stimulated biological activity (Lucas et al., 2021). A well-connected macropore system typically facilitates aeration as well as water and matter fluxes. We observed that the unsaturated hydraulic conductivity at field capacity decreased with increasing bulk density. However, the variability among replicates was high and disguised any potential trends with FYM application. Except for situations when the soil is close to saturation, the macropore system (>38 μm) is not involved in water flow or water storage, since such pores of low capillarity are filled with air. Under unsaturated conditions, soil texture and OC are supposed to have a major influence on hydraulic properties. Nevertheless, the observed increase in TOC was neither accompanied by an increase in unsaturated hydraulic conductivity, in PAWC, nor in a shift of the permanent wilting point. Hati et al. (2006) observed similar results, with no significant impact of FYM application on hydraulic conductivity of soil below 22.5 cm depth. This is in contrast to previous studies reporting positive effects of increased TOC on hydraulic soil properties (Bhattacharyya et al., 2007; Ozlu et al., 2019). However, most studies measured the effect of increased TOC only for ploughed layers and/or saturated conditions, when the macropore system, which is directly affected by FYM-derived coarse POM, is of greater relevance and stability against slaking and settling is more relevant. In this study, the positive effect of FYM on subsoil's macropore system and TOC was not sufficient to be reflected in changes in the soil water retention curve of the subsoil. Our results are supported by the meta-analysis of Minasny and McBratney (2018), who questioned the effect of OC on water retention over a broad range of matrix potentials and soil textures. It is shown that the overall effect of OC on soil water retention is small and decreases with increasing water suction and increasing contents of fined textured material. Also Tóth et al. (2015) showed for pedotransfer functions that soil texture is the most important factor of soil water retention and that OC is predominantly an indicator for differences in related physico-chemical soil properties, including soil structure.

4.4 | Minor effect of long-term FYM application on maize yield but high environmental impact

Over the last 25 years, maize yield increased by about 25% relative to control independent from the FYM application rate (Figure S3). Seemingly, application of 50 Mg FYM ha^{-1} a^{-1} already provides sufficient supply of nutrients and the determined differences in subsoil TOC and hydraulic properties induced by the larger rates lend no additional support to increased plant productivity. Since the study site is located in an area with low annual rainfall (480 mm) and periods of drought, the limitation in water might have prevented potential differences in yield between the FYM application rates and at the same time stimulated root growth to greater depth. The application rates all well exceed those recommended for the study site (20 Mg FYM ha^{-1} every second year in combination with NPK fertilisation (Merbach & Schulz, 2013)) and more than three times the maximum allowable amount of OC input according to the German Decision Support System for soil C stock balancing (Franko & Schulz, 2021). This shows that FYM application rates that are required to induce OC accumulation in arable subsoil are beyond common agricultural practice and available resources. Also, such high application rates pose high risks to the environment. Since most of the extra C entering the subsoil is labile fresh POM, long-term storage is unlikely, and most of it will be released into the atmosphere soon. In addition, the applied FYM rates provides N far beyond the demand of crops. This poses the risk of increased emissions of gaseous N, especially of the potent greenhouse gas N_2O (Cui et al., 2021), and leaching of NO_3^- into groundwater. In summary, the applied FYM rates are not suitable for a sustainable land use, which supports the limitations of FYM application for C storage in soil outlined by Poulton et al. (2018).

5 | CONCLUSION

Long-term (36 years), high-rate application of FYM increased OC and TN contents in ploughed soil layer as well as the subsoil. Much of the C input to subsoil was brought about by fresh POM via roots and vertical transport of plant and FYM residues most probably by megafauna activity. Our observation indicates that a minimum FYM application rate of 100 Mg ha^{-1} a^{-1} (938 kg C m^{-2} a^{-1}) for 36 years was required to trigger enrichment of OC in the subsoil at the study site, since no increase was found at a rate of 50 Mg ha^{-1} a^{-1} (469 kg C m^{-2} a^{-1}). However, these rates are well above common agricultural practices and entail a high risk for the environment due to C and N losses. The increase in WEOC in the topsoils with increasing FYM doses did not translate into largely differing MAOM concentrations in the subsoil. Consequently, it is unlikely that this mobile fraction was a major source for subsoil MAOM under these dry climatic conditions. We therefore conclude that the contribution of soluble organic matter to subsoil OC was far smaller than that of POM.

Decomposed POM was mainly located in areas with long distances to the next macropore, indicating possible stabilisation by occlusion within the mineral matrix. The preferential accumulation of fresh, labile POM in response to large application rates of FYM questions the potential of arable subsoils for long-term storage of C for this combination of soil type and site conditions.

Based on the results presented herein, it was shown that:

1. The vertical C translocation was increasing with FYM application rate, but the increase in subsoil OC content was not concomitant to the increase in FYM-C input.
2. The increase in subsoil TOC was accompanied by an increase in visible porosity for pores with a diameter of 38–140 μm, an increase in pore connectivity and a decrease in pore distance.
3. The increase in TOC content and the change in soil structure did not affect the plant-available water capacity and the unsaturated conductivity of the subsoil as hypothesised.

ACKNOWLEDGEMENT

We would like to thank Bernd Apelt, Alexandra Boritzki, Christine Krenkewitz and Anja Kroner for their help and support with the laboratory work.

Open access funding enabled and organized by Projekt DEAL. Open access funding enabled and organized by Projekt DEAL.

CONFLICT OF INTEREST

The authors declare that they have no conflict of interest.

AUTHOR CONTRIBUTIONS

Frederic Leuther: Conceptualisation (lead); data curation (lead); formal analysis (lead); investigation (equal); methodology (lead); validation (lead); visualisation (lead); writing–original draft (lead); writing–review and editing (lead). **Maximilian Wolff:** Conceptualization (equal); data curation (equal); formal analysis (equal); investigation (equal); methodology (equal); writing – original draft (equal). **Klaus Kaiser:** Conceptualization (supporting); formal analysis (supporting); funding acquisition (equal); methodology (equal); writing – original draft (supporting). **Lena Schumann:** Data curation (supporting); formal analysis (supporting); writing – original draft (supporting). **Ines Merbach:** Data curation (supporting); writing – original draft (supporting). **Robert Mikutta:** Conceptualization (supporting); funding acquisition (equal); methodology (supporting); project administration (equal); supervision (equal); writing – original draft (supporting). **Steffen Schlüter:** Conceptualization (equal); formal analysis (supporting); funding acquisition (equal); investigation (supporting); methodology (supporting); supervision (equal); visualization (supporting); writing – original draft (supporting).

DATA AVAILABILITY STATEMENT

All data are available within the article and in the supplement. Segmented and classified (POM) X-ray μCT images and the structural characteristics of the pore network are provided online: https://www.ufz.de/record/dmp/archive/11882/de/#download

ORCID

Frederic Leuther https://orcid.org/0000-0001-6955-7892
Maximilian Wolff https://orcid.org/0000-0003-0226-7246
Klaus Kaiser https://orcid.org/0000-0001-7376-443X
Robert Mikutta https://orcid.org/0000-0002-7186-6528
Steffen Schlüter https://orcid.org/0000-0002-3140-9058

REFERENCES

Altermann, M., Rinklebe, J., Merbach, I., Körschens, M., Langer, U., & Hofmann, B. (2005). Chernozem—Soil of the year 2005. *Journal of Plant Nutrition and Soil Science*, *168*, 725–740.

Andersen, N. (1983). Nitrogen turnover by earthworms in arable plots treated with farmyard manure and slurry. In *Earthworm ecology* (pp. 139–150). Springer.

Angst, G., Mueller, C. W., Prater, I., Angst, Š., Frouz, J., Jílková, V., Peterse, F., & Nierop, K. G. (2019). Earthworms act as biochemical reactors to convert labile plant compounds into stabilized soil microbial necromass. *Communications Biology*, *2*, 1–7.

Batjes, N. H. (2014). Total carbon and nitrogen in the soils of the world. *European Journal of Soil Science*, *65*, 10–21.

Benbi, D., Biswas, C., Bawa, S., & Kumar, K. (1998). Influence of farmyard manure, inorganic fertilizers and weed control practices on some soil physical properties in a long-term experiment. *Soil Use and Management*, *14*, 52–54.

Berg, S., Kutra, D., Kroeger, T., Straehle, C. N., Kausler, B. X., Haubold, C., Schiegg, M., Ales, J., Beier, T., Rudy, M., Eren, K., Cervantes, J. I., Xu, B., Beuttenmueller, F., Wolny, A., Zhang, C., Koethe, U., Hamprecht, F. A., & Kreshuk, A. (2019). Ilastik: Interactive machine learning for (bio)image analysis. *Nature Methods*, *16*, 1226–1232.

Bhattacharyya, R., Chandra, S., Singh, R., Kundu, S., Srivastva, A., & Gupta, H. (2007). Long-term farmyard manure application effects on properties of a silty clay loam soil under irrigated wheat–soybean rotation. *Soil and Tillage Research*, *94*, 386–396.

Buades, A., Coll, B., & Morel, J.-M. (2011). Non-local means denoising. *Image Processing On Line*, *1*, 208–212.

Chen, S., Arrouays, D., Angers, D. A., Martin, M. P., & Walter, C. (2019). Soil carbon stocks under different land uses and the applicability of the soil carbon saturation concept. *Soil and Tillage Research*, *188*, 53–58.

Comas, L., Becker, S., Cruz, V. M., Byrne, P. F., & Dierig, D. A. (2013). Root traits contributing to plant productivity under drought. *Frontiers in Plant Science*, *4*(442), 442.

Cui, X., Zhou, F., Ciais, P., Davidson, E. A., Tubiello, F. N., Niu, X., Ju, X., Canadell, J. G., Bouwman, A. F., Jackson, R. B., Mueller, N. D., Zheng, X., Kanter, D. R., Tian, H., Adalibieke, W., Bo, Y., Wang, Q., Zhan, X., & Zhu, D. (2021). Global mapping of crop-specific emission factors highlights hotspots of nitrous oxide mitigation. *Nature Food.*, *2*, 886–893.

Dal Ferro, N., Charrier, P., & Morari, F. (2013). Dual-scale micro-CT assessment of soil structure in a long-term fertilization experiment. *Geoderma*, *204-205*, 84–93.

Dal Ferro, N., Sartori, L., Simonetti, G., Berti, A., & Morari, F. (2014). Soil macro- and microstructure as affected by different tillage systems and their effects on maize root growth. *Soil and Tillage Research*, *140*, 55–65.

de Mendiburu, F. (2019). *Package 'agricolae'* (pp. 1–2). R Package.

de Moraes, M. T., Debiasi, H., Franchini, J. C., Bonetti, J.d. A., Levien, R., Schnepf, A., & Leitner, D. (2019). Mechanical and hydric stress effects on maize root system development at different soil compaction levels. *Frontiers in Plant Science*, *10*, 1358.

Dreibrodt, S., Kleber, M., & Jahn, R. (2002). Das Mineralinventar der Versuchsfläche "Statischer Dauerdüngungsversuch V120, Bad Lauchstädt". *Archives of Agronomy and Soil Science*, *48*, 227–240.

Dungait, J. A., Hopkins, D. W., Gregory, A. S., & Whitmore, A. P. (2012). Soil organic matter turnover is governed by accessibility not recalcitrance. *Global Change Biology*, *18*, 1781–1796.

Ekschmitt, K., Kandeler, E., Poll, C., Brune, A., Buscot, F., Friedrich, M., Gleixner, G., Hartmann, A., Kästner, M., & Marhan, S. (2008). Soil-carbon preservation through habitat constraints and biological limitations on decomposer activity. *Journal of Plant Nutrition and Soil Science*, *171*, 27–35.

Elyeznasni, N., Sellami, F., Pot, V., Benoit, P., Vieublé-Gonod, L., Young, I., & Peth, S. (2012). Exploration of soil micromorphology to identify coarse-sized OM assemblages in X-ray CT images of undisturbed cultivated soil cores. *Geoderma*, *179-180*, 38–45.

Franko, U., & Schulz, E. (2021). Carbon accumulation in a bare fallow Chernozem soil with high carbon input rates. *European Journal of Soil Science*, *72*, 265–273.

Gajri, P., Arora, V., & Chaudhary, M. (1994). Maize growth responses to deep tillage, straw mulching and farmyard manure in coarse textured soils of NW India. *Soil Use and Management*, *10*, 15–19.

Ghosh, A., Bhattacharyya, R., Meena, M., Dwivedi, B., Singh, G., Agnihotri, R., & Sharma, C. (2018). Long-term fertilization effects on soil organic carbon sequestration in an Inceptisol. *Soil and Tillage Research*, *177*, 134–144.

Golchin, A., Oades, J., Skjemstad, J., & Clarke, P. (1994). Study of free and occluded particulate organic matter in soils by solid state 13C CP/MAS NMR spectroscopy and scanning electron microscopy. *Soil Research*, *32*, 285–309.

Grosbellet, C., Vidal-Beaudet, L., Caubel, V., & Charpentier, S. (2011). Improvement of soil structure formation by degradation of coarse organic matter. *Geoderma*, *162*, 27–38.

Gross, A., & Glaser, B. (2021). Meta-analysis on how manure application changes soil organic carbon storage. *Scientific Reports*, *11*, 1–13.

Hati, K., Mandal, K., Misra, A., Ghosh, P., & Bandyopadhyay, K. (2006). Effect of inorganic fertilizer and farmyard manure on soil physical properties, root distribution, and water-use efficiency of soybean in Vertisols of Central India. *Bioresource Technology*, *97*, 2182–2188.

Hudson, B. D. (1994). Soil organic matter and available water capacity. *Journal of Soil and Water Conservation*, *49*, 189–194.

Jarvis, N., Larsbo, M., & Koestel, J. (2017). Connectivity and percolation of structural pore networks in a cultivated silt loam soil quantified by X-ray tomography. *Geoderma*, *287*, 71–79.

Jarvis, N. J. (2007). A review of non-equilibrium water flow and solute transport in soil macropores: Principles, controlling factors and consequences for water quality. *European Journal of Soil Science*, *58*, 523–546.

John, B., Yamashita, T., Ludwig, B., & Flessa, H. (2005). Storage of organic carbon in aggregate and density fractions of silty soils under different types of land use. *Geoderma*, *128*, 63–79.

Juyal, A., Guber, A., Oerther, M., Quigley, M., & Kravchenko, A. (2021). Pore architecture and particulate organic matter in soils under monoculture switchgrass and restored prairie in contrasting topography. *Scientific Reports*, *11*, 21998.

Kaiser, K., Eusterhues, K., Rumpel, C., Guggenberger, G., & Kögel-Knabner, I. (2002). Stabilization of organic matter by soil minerals—Investigations of density and particle-size fractions from two acid forest soils. *Journal of Plant Nutrition and Soil Science*, *165*, 451–459.

Kaiser, K., & Kalbitz, K. (2012). Cycling downwards–dissolved organic matter in soils. *Soil Biology and Biochemistry*, *52*, 29–32.

Kassambara, A. 2020. rstatix: pipe-friendly framework for basic statistical tests. R package version 0.4. 0. Avaliable online at: https://cran.r-project.org/web/packages/rstatix/index

Körschens, M., Schulz, E., & Knappe, S. (1994). Von Dauerbrache und Fruchtfolge auf die N-Bilanzen einer Löss-Schwarzerde unter Berücksichtigung extremer Düngungsvarianten. *Archives of Agronomy and Soil Science*, *38*, 415–422.

Kravchenko, A., Guber, A., Razavi, B., Koestel, J., Quigley, M., Robertson, G., & Kuzyakov, Y. (2019). Microbial spatial footprint as a driver of soil carbon stabilization. *Nature Communications*, *10*, 1–10.

Lal, R. (2018). Digging deeper: A holistic perspective of factors affecting soil organic carbon sequestration in agroecosystems. *Global Change Biology*, *24*, 3285–3301.

Legland, D., Arganda-Carreras, I., & Andrey, P. (2016). MorphoLibJ: Integrated library and plugins for mathematical morphology with ImageJ. *Bioinformatics*, *32*, 3532–3534.

Lehmann, J., & Kleber, M. (2015). The contentious nature of soil organic matter. *Nature*, *528*, 60–68.

Liang, Q., Chen, H., Gong, Y., Fan, M., Yang, H., Lal, R., & Kuzyakov, Y. (2012). Effects of 15 years of manure and inorganic fertilizers on soil organic carbon fractions in a wheat-maize system in the North China plain. *Nutrient Cycling in Agroecosystems*, *92*, 21–33.

Liaw, A., & Wiener, M. (2002). Classification and regression by randomForest. *R News*, *2*, 18–22.

Lucas, M., Schlüter, S., Vogel, H.-J., & Vetterlein, D. (2019). Soil structure formation along an agricultural chronosequence. *Geoderma*, *350*, 61–72.

Lucas, M., Vetterlein, D., Vogel, H.-J., & Schlüter, S. (2021). Revealing pore connectivity across scales and resolutions with X-ray CT. *European Journal of Soil Science*, *72*, 546–560.

Masood, S., Naz, T., Javed, M. T., Ahmed, I., Ullah, H., & Iqbal, M. (2014). Effect of short-term supply of farmyard manure on maize growth and soil parameters in pot culture. *Archives of Agronomy and Soil Science*, *60*, 337–347.

Mehra, O., & Jackson, M. (1960). Iron oxide removal from soils and clays by a dithionite–citrate system buffered with sodium bicarbonate. *Clays and Clay Minerals*, *7*, 317–327.

Merbach, I., & Schulz, E. (2013). Long-term fertilization effects on crop yields, soil fertility and sustainability in the static fertilization experiment Bad Lauchstädt under climatic conditions 2001–2010. *Archives of Agronomy and Soil Science*, *59*, 1041–1057.

Mikutta, R., Turner, S., Schippers, A., Gentsch, N., Meyer-Stüve, S., Condron, L. M., Peltzer, D. A., Richardson, S. J., Eger, A., & Hempel, G. (2019). Microbial and abiotic controls on mineral-associated organic matter in soil profiles along an ecosystem gradient. *Scientific Reports*, *9*, 1–9.

Minasny, B., & McBratney, A. (2018). Limited effect of organic matter on soil available water capacity. *European Journal of Soil Science*, *69*, 39–47.

Moody, C., & Worrall, F. (2017). Modeling rates of DOC degradation using DOM composition and hydroclimatic variables. *Journal of Geophysical Research: Biogeosciences*, *122*, 1175–1191.

Otsu, N. (1979). A threshold selection method from gray-level histograms. *IEEE Transactions on Systems, Man, and Cybernetics*, *9*, 62–66.

Ozlu, E., Kumar, S., & Arriaga, F. J. (2019). Responses of long-term cattle manure on soil physical and hydraulic properties under a corn-soybean rotation at two locations in eastern South Dakota. *Soil Science Society of America Journal*, *83*, 1459–1467.

Poulton, P., Johnston, J., Macdonald, A., White, R., & Powlson, D. (2018). Major limitations to achieving "4 per 1000" increases in soil organic carbon stock in temperate regions: Evidence from long-term experiments at Rothamsted Research, United Kingdom. *Global Change Biology*, *24*, 2563–2584.

R Core Team. (2020). *R: A language and environment for statistical computing*. Austria.

Rabot, E., Wiesmeier, M., Schlüter, S., & Vogel, H.-J. (2018). Soil structure as an indicator of soil functions: A review. *Geoderma*, *314*, 122–137.

Renard, P., & Allard, D. (2013). Connectivity metrics for subsurface flow and transport. *Advances in Water Resources*, *51*, 168–196.

Robinson, D. (2007). Implications of a large global root biomass for carbon sink estimates and for soil carbon dynamics. *Proceedings of the Royal Society B: Biological Sciences*, *274*, 2753–2759.

Rumpel, C., Chabbi, A., & Marschner, B. (2012). Carbon storage and sequestration in subsoil horizons: Knowledge, gaps and potentials. In *Recarbonization of the biosphere* (pp. 445–464). Springer.

Rumpel, C., & Kögel-Knabner, I. (2011). Deep soil organic matter—A key but poorly understood component of terrestrial C cycle. *Plant and Soil*, *338*, 143–158.

Scharlemann, J. P., Tanner, E. V., Hiederer, R., & Kapos, V. (2014). Global soil carbon: Understanding and managing the largest terrestrial carbon pool. *Carbon Management*, *5*, 81–91.

Schindelin, J., Arganda-Carreras, I., Frise, E., Kaynig, V., Longair, M., Pietzsch, T., Preibisch, S., Rueden, C., Saalfeld, S., Schmid, B., Tinevez, J.-Y., White, D. J., Hartenstein, V., Eliceiri, K., Tomancak, P., & Cardona, A. (2012). Fiji: An open-source platform for biological-image analysis. *Nature Methods*, *9*, 676–682.

Schindler, U., Durner, W., von Unold, G., & Müller, L. (2010). Evaporation method for measuring unsaturated hydraulic properties of soils: Extending the measurement range. *Soil Science Society of America Journal*, *74*, 1071–1083.

Schjønning, P., Christensen, B. T., & Carstensen, B. (1994). Physical and chemical properties of a sandy loam receiving animal manure, mineral fertilizer or no fertilizer for 90 years. *European Journal of Soil Science*, *45*, 257–268.

Schlüter, S., Großmann, C., Diel, J., Wu, G.-M., Tischer, S., Deubel, A., & Rücknagel, J. (2018). Long-term effects of conventional and reduced tillage on soil structure, soil ecological and soil hydraulic properties. *Geoderma*, *332*, 10–19.

Schlüter, S., Leuther, F., Vogler, S., & Vogel, H. J. (2016). X-ray microtomography analysis of soil structure deformation caused by centrifugation. *Solid Earth*, *7*, 129–140.

Schlüter, S., Leuther, F., Albrecht, L., Hoeschen, C., Kilian, R., Surey, R., Mikutta, R., Kaiser, K., Mueller, C., & Vogel, H.-J. (2022). Microscale carbon distribution around pores and particulate organic matter varies with soil moisture regime. *Nature Communications*, (Accepted).

Schwertmann, U. (1964). Differenzierung der Eisenoxide des Bodens durch Extraktion mit Ammoniumoxalat-Lösung. *Zeitschrift für Pflanzenernährung, Düngung, Bodenkunde*, *105*, 194–202.

Shahzad, H., Ullah, S., & Iqbal, M. (2014). Effect of various farm manure levels on root proliferation and maize growth under different soil textures. *International Journal of Modern Agriculture*, *3*, 106–115.

Singh, N., Kumar, S., Udawatta, R., Anderson, S., Jonge, L., & Katuwal, S. (2021). X-ray micro-computed tomography characterized soil pore network as influenced by long-term application of manure and fertilizer. *Geoderma*, *385*, 114872.

Six, J., Bossuyt, H., Degryze, S., & Denef, K. (2004). A history of research on the link between (micro) aggregates, soil biota, and soil organic matter dynamics. *Soil and Tillage Research*, *79*, 7–31.

Surey, R., Lippold, E., Heilek, S., Sauheitl, L., Henjes, S., Horn, M. A., Mueller, C. W., Merbach, I., Kaiser, K., & Böttcher, J. (2020). Differences in labile soil organic matter explain potential denitrification and denitrifying communities in a long-term fertilization experiment. *Applied Soil Ecology*, *153*, 103630.

Tóth, B., Weynants, M., Nemes, A., Makó, A., Bilas, G., & Tóth, G. (2015). New generation of hydraulic pedotransfer functions for Europe. *European Journal of Soil Science*, *66*, 226–238.

Vogel, H. J., Weller, U., & Schlüter, S. (2010). Quantification of soil structure based on Minkowski functions. *Computers & Geosciences*, *36*, 1236–1245.

Weller, U., Albrecht, L., Schlüter, S., & Vogel, H. J. (2021). An open soil structure library based on X-ray CT data. *Soil Discussion*, *2021*, 1–13.

Wickham, H. (2016). *ggplot2: Elegant graphics for data analysis*. Springer.

Wickham, H., Averick, M., Bryan, J., Chang, W., McGowan, L. D. A., François, R., Grolemund, G., Hayes, A., Henry, L., & Hester, J. (2019). Welcome to the Tidyverse. *Journal of Open Source Software*, *4*, 1686.

Wiesmeier, M., Urbanski, L., Hobley, E., Lang, B., von Lützow, M., Marin-Spiotta, E., van Wesemael, B., Rabot, E., Ließ, M., Garcia-Franco, N., Wollschläger, U., Vogel, H.-J., & Kögel-Knabner, I. (2019). Soil organic carbon storage as a key function of soils - a review of drivers and indicators at various scales. *Geoderma*, *333*, 149–162.

Witzgall, K., Vidal, A., Schubert, D. I., Höschen, C., Schweizer, S. A., Buegger, F., Pouteau, V., Chenu, C., & Mueller, C. W. (2021). Particulate organic matter as a functional soil component for persistent soil organic carbon. *Nature Communications*, *12*, 1–10.

Zhang, X., Neal, A. L., Crawford, J. W., Bacq-Labreuil, A., Akkari, E., & Rickard, W. (2021). The effects of long-term fertilizations on soil hydraulic properties vary with scales. *Journal of Hydrology*, *593*, 125890.

SUPPORTING INFORMATION

Additional supporting information may be found in the online version of the article at the publisher's website.

How to cite this article: Leuther, F., Wolff, M., Kaiser, K., Schumann, L., Merbach, I., Mikutta, R., & Schlüter, S. (2022). Response of subsoil organic matter contents and physical properties to long-term, high-rate farmyard manure application. *European Journal of Soil Science*, *73*(2), e13233. https://doi.org/10.1111/ejss.13233